Utility of Thin-slice Fat-suppressed Single-shot T2-weighted MR Imaging with Deep Learning Image Reconstruction as a Protocol for Evaluating the Pancreas

Shimada, Ryuji ; Sofue, Keitaro ; Ueno, Yoshiko ; Wakayama, Tetsuya ; Yamaguchi, Takeru ; Ueshima, Eisuke ; Kusaka, Akiko ; Hori, Masatoshi ⋯

(Citation)
Magnetic Resonance in Medical Sciences:1-10

(Issue Date)
2024-06-21

(Resource Type)
journal article

(Version)
Version of Record

Magn Reson Med Sci
doi:10.2463/mrms.mp.2024-0017 Published Online: June 21, 2024

MAJOR PAPER

Utility of Thin-slice Fat-suppressed Single-shot T2-weighted MR Imaging with Deep Learning Image Reconstruction as a Protocol for Evaluating the Pancreas

Ryuji Shimada[1,2], Keitaro Sofue[1*], Yoshiko Ueno[1], Tetsuya Wakayama[3], Takeru Yamaguchi[1], Eisuke Ueshima[1], Akiko Kusaka[2], Masatoshi Hori[1], and Takamichi Murakami[1]

Purpose: To compare the utility of thin-slice fat-suppressed single-shot T2-weighted imaging (T2WI) with deep learning image reconstruction (DLIR) and conventional fast spin-echo T2WI with DLIR for evaluating pancreatic protocol.

Methods: This retrospective study included 42 patients (mean age, 70.2 years) with pancreatic cancer who underwent gadoxetic acid-enhanced MRI. Three fat-suppressed T2WI, including conventional fast-spin echo with 6 mm thickness (FSE 6 mm), single-shot fast-spin echo with 6 mm and 3 mm thickness (SSFSE 6 mm and SSFSE 3 mm), were acquired for each patient. For quantitative analysis, the SNRs of the upper abdominal organs were calculated between images with and without DLIR. The pancreas-to-lesion contrast on DLIR images was also calculated. For qualitative analysis, two abdominal radiologists independently scored the image quality on a 5-point scale in the FSE 6 mm, SSFSE 6 mm, and SSFSE 3 mm with DLIR.

Results: The SNRs significantly improved among the three T2-weighted images with DLIR compared to those without DLIR in all patients ($P < 0.001$). The pancreas-to-lesion contrast of SSFSE 3 mm was higher than those of the FSE 6 mm ($P < 0.001$) and tended to be higher than SSFSE 6 mm ($P = 0.07$). SSFSE 3 mm had the highest image qualities regarding pancreas edge sharpness, pancreatic duct clarity, and overall image quality, followed by SSFSE 6 mm and FSE 6 mm ($P < .0001$).

Conclusion: SSFSE 3 mm with DLIR demonstrated significant improvements in SNRs of the pancreas, pancreas-to-lesion contrast, and image quality more efficiently than did SSFSE 6 mm and FSE 6 mm. Thin-slice fat-suppressed single-shot T2WI with DLIR can be easily implemented for pancreatic MR protocol.

Keywords: *artificial intelligence, magnetic resonance imaging, pancreas, T2-weighted*

Introduction

T2-weighted imaging (T2WI) is an essential sequence in abdominal MRI. A 2D fast spin-echo (FSE) T2WI sequence with fat suppression is routinely used to acquire T2WI of the abdomen, which provides sufficient spatial resolution and SNR.[1,2] However, 2D FSE T2WI requires respiratory triggered or multiple breath-hold acquisitions, resulting in relatively higher motion artifacts, blurring, and longer acquisition time.[1–3] Despite several attempts, such as using rotated overlapping parallel lines and 3D FSE pulse sequences, to enhance image quality, routine clinical utilization has been hindered by the emergence of increased streak artifacts, B1 inhomogeneity, and reduced SNR.[4,5]

The single-shot fast-spin echo (SSFSE) sequence can be obtained as a supplemental sequence for FSE T2WI of the abdomen. It acquires the entire k-space data for each image with a single radiofrequency excitation, followed by multiple refocusing radiofrequency pulses. The SSFSE is intrinsically

[1]Department of Radiology, Kobe University Graduate School of Medicine, Kobe, Hyogo, Japan
[2]Center for Radiology and Radiation Oncology, Kobe University Hospital, Kobe, Hyogo, Japan
[3]MR Collaborations and Development, GE Healthcare, Hino, Tokyo, Japan
*Corresponding author: Department of Radiology, Kobe University Graduate School of Medicine, 7-5-2, Kusunoki-cho, Chuo-ku, Kobe, Hyogo 650-0017, Japan. Phone: +81-78-382-6104, E-mail: keitarosofue@gmail.com

Received: February 4, 2024 | Accepted: May 14, 2024

fast and robust to motion corruption, significantly reducing acquisition time and motion artifacts.[6] Recent technical developments have facilitated high-resolution SSFSE using a shortened echo space period, high parallel imaging factor, and extended echo train length with the modulation of variable refocusing flip angles.[7,8] In contrast, the single-shot pulse sequence can potentially decrease the SNR and lesion conspicuity caused by T2 decay.[9] Another drawback is that the ghosting artifacts from the high signal intensity of intraperitoneal fat may affect the lesion conspicuity; however, fat suppression increases the acquisition time and deteriorates the image quality.[9,10] In pancreatic MRI, conventional FSE and SSFSE sequences without fat suppression are used to evaluate the focal lesions, pancreatic duct continuity, pancreatic shape, and liver metastases.[11] However, fast and robust fat-suppressed T2WI, which achieves a high SNR and spatial resolution, is anticipated as an alternative to conventional T2WI.

The deep learning image reconstruction (DLIR) has recently been introduced to accelerate acquisition time and reduce image noise without compromising the image contrast.[12–18] The clinical usefulness of DLIR for single-shot T2WI has been reported in the liver, and single-shot T2WI with DLIR has improved the image quality and lesion conspicuity with a reduction in acquisition time.[15–17] Thus, we hypothesized that thin-slice fat-suppressed single-shot T2WI with DLIR would improve the image quality of the pancreas and lesion conspicuity in pancreatic cancer. This study aimed to investigate the utility of thin-slice fat-suppressed single-shot T2WI with DLIR for the evaluation of pancreatic cancer compared to that of conventional fast spin-echo T2WI with DLIR.

Materials and Methods

Patients

This study was a single-institution retrospective analysis of a prospectively collected cohort and was approved by Ethics Committee of Kobe University Hospital (B220245). The need for written informed consent was waived by the review board. One of the authors was an employee of GE Healthcare; however, the author did not have control over any of the data or information submitted for publication or over which data and information were to be included in this study.

Overall, 42 consecutive patients (27 males and 15 females; mean age, 70.2 ± 10.8 years; range, 43–90 years) with pancreatic cancer underwent gadoxetic-acid enhanced MRI between January 2021 and September 2022. Forty-two pancreatic ductal adenocarcinomas (pancreatic head [n = 31] and body/tail [n = 11]) in 42 patients were confirmed by histopathological examination using endoscopic ultrasonography-guided biopsy followed by surgical resection. None of the patients had undergone surgery, chemotherapy, or radiation therapy for pancreatic cancer prior to the MRI examination.

MRI examination

All MRI examinations were performed using a 3T MR scanner (SIGNA Premier; GE Healthcare, Hino, Japan) with a 21-channel multipurpose anterior array coil and a table-embedded 60-channel posterior array coil. Three fat-suppressed T2WI, including conventional FSE with 6 mm thickness (FSE 6 mm), SSFSE with 6 mm thickness (SSFSE 6 mm), and SSFSE with 3 mm thickness (SSFSE 3 mm), were acquired for each patient. The three T2-weighted sequences were consecutively imaged 3 mins after injecting gadoxetic acid (Primovist; Bayer Pharma, Osaka, Japan) while waiting to acquire hepatobiliary phase images. The scan order for the three T2-weighted sequences was randomized to avoid timing bias of the T2 shortening effect caused by the gadoxetic acid contrast agent. The number of breath-holds of the FSE 6 mm, SSFSE 6 mm, and SSFSE 3 mm was set to three, one, and two, respectively, covering all upper abdominal organs, including the liver and pancreas. For SSFSE, a variable refocusing flip angle and a parallel imaging acceleration factor of three were applied to minimize the T2 decay. The full-Fourier acquisition was used to achieve image sharpness and appropriate TEs relevant for evaluating abdominal organs.[7,14] The detailed scan parameters of the three sequences are listed in Table 1.

A commercially available DLIR algorithm (AIR Recon DL; GE Healthcare), consisting of a deep convolutional neural network trained with a supervised learning approach using pairs of near-perfect and conventional MRI images, was used. The network replaced a traditional k-space filter to achieve a higher SNR and sharper image with reduced truncation artifacts compared with those of a conventional reconstruction using a k-space filter.[19] The DLIR network was embedded in the conventional reconstruction pathway, and two sets of images were reconstructed from a single raw data set. Importantly, a different convolutional neural network application strength (low, medium, and high) must be set to generate images before image acquisition. In this study, the three T2-weighted sequences obtained were reconstructed without DLIR and with high-strength DLIR for image analyses.

Quantitative image analysis

Quantitative image analysis was performed by a radiologic technician (R.S.) and a board-certified abdominal radiologist (E.U.; 15 years of experience in abdominal imaging) in consensus. Oval ROIs were placed in the right and left liver lobes, pancreas, pancreatic cancer, paraspinal muscle, and intra-abdominal fat to measure the signal intensity (SI) and standard deviation (SD) (Fig. 1). The ROIs were as large as possible for each object. The ROIs of the liver were placed to avoid intrahepatic vasculature or focal liver lesions. The ROI of the pancreas was placed proximal to the tumor to exclude the area of high SI, which is peripheral edema caused by pancreatic duct obstruction in pancreatic cancer. All quantitative measurements in each tissue were performed twice to confirm data consistency, and the average values were used for the analyses.

Table 1 Acquisition parameters on the three T2-weighted sequences

Sequence/T2WI	FSE 6 mm	SSFSE 6 mm	SSFSE 3 mm
Scan plane	Axial	Axial	Axial
Shot mode	Multi-shot	Single-shot	Single-shot
Freq FOV (cm)/phase FOV	32 40/0.8	32 40/0.8	32 40/0.8
Slice thickness/spacing (mm)	6/0	6/0	3/0
Slices	34	34	68
TR (ms)	2200	Minimum	Minimum
TE (ms)	80	78 (minfull)	80 (minfull)
Flip angle (degree)	100	VRFA	VRFA
Data acquisition	Full-Fourier	Full-Fourier	Full-Fourier
Frequency direction	R-L	A-P	A-P
Parallel imaging	ARC 2.0	ASSET 3.0	ASSET 3.0
Recon DL strength	High	High	High
Matrix (frequency × phase)	440 × 240	512 × 144	512 × 144
Bandwidth (±kHz)	100	125	111
Echo spacing (msec)	6.2	4.1	4.3
Slice ordering	Interleave	Interleave	Interleave
Chemical saturation	Fat	Special	Special
Breath hold instructions	Exhalation	Exhalation	Exhalation
Breath hold (sec) × times	16 × 3	16 × 1	16 × 2

ARC, auto-calibrating reconstruction for Cartesian imaging; ASSET, array spatial sensitivity encoding technique; FSE, fast spin echo; SSFSE, single-shot fast spin echo; T2WI, T2-weighted imaging; VRFA, variable refocusing flip angle.

The SNR for each object was calculated for the images with and without DLIR using equation (1):

$$\mathrm{SNR} = \mathrm{SI}_{\mathrm{Object}}/\mathrm{SD}_{\mathrm{Object}}, \quad (1)$$

where $\mathrm{SI}_{\mathrm{Object}}$ and $\mathrm{SD}_{\mathrm{Object}}$ represent the mean SI and SD of each object, respectively.

The percentage increase in the SNR by applying DLIR (SNR increase%) was calculated for each object using equation (2):

$$\text{SNR increase } \% = (\mathrm{SNR}_{\mathrm{DL+}}/\mathrm{SNR}_{\mathrm{DL-}}) \times 100, \quad (2)$$

where $\mathrm{SNR}_{\mathrm{DL+}}$ and $\mathrm{SNR}_{\mathrm{DL-}}$ represent the SNR calculated from the images with and without DLIR, respectively.

The pancreas-to-lesion contrast on the DLIR images was calculated using equation (3):

$$\text{Pancreas-to-lesion contrast} = (\mathrm{SI}_{\mathrm{Lesion}} - \mathrm{SI}_{\mathrm{Pancreas}})/\mathrm{SI}_{\mathrm{Pancreas}} \quad (3)$$

where $\mathrm{SI}_{\mathrm{Lesion}}$ and $\mathrm{SI}_{\mathrm{Pancreas}}$ represent the SI of pancreatic cancer and pancreas, respectively.

The pancreas-to-lesion contrast was evaluated only on the DLIR images, because signal intensity did not change between the images without and with DLIR in the previous paper.[20]

Qualitative image analysis

Two board-certified radiologists independently performed qualitative image analysis (K.S. and Y.U. with 21 and 17 years of experience in abdominal imaging, respectively). They were blinded to the information about the images; however, they were informed of the presence and location of pancreatic cancer. We evaluated three DLIR sequence images rather than images without DLIR, because each T2-weighted image with DLIR achieved significantly higher SNR than that without DLIR in all the objects (see Results section) and thought to be clinically feasible. Three DLIR sequence images were evaluated for subjective image quality, including respiratory motion artifacts, pancreatic edge sharpness, pancreatic duct clarity, lesion conspicuity, fat suppression homogeneity, and overall image quality. Respiratory motion artifacts were evaluated using a 5-point scale (1 = non-diagnostic because of severe artifacts; 2 = moderate artifacts affecting diagnosis; 3 = mild artifacts; 4 = minimal artifacts; 5 = no artifacts). Pancreatic edge sharpness, pancreatic duct clarity, lesion conspicuity, fat

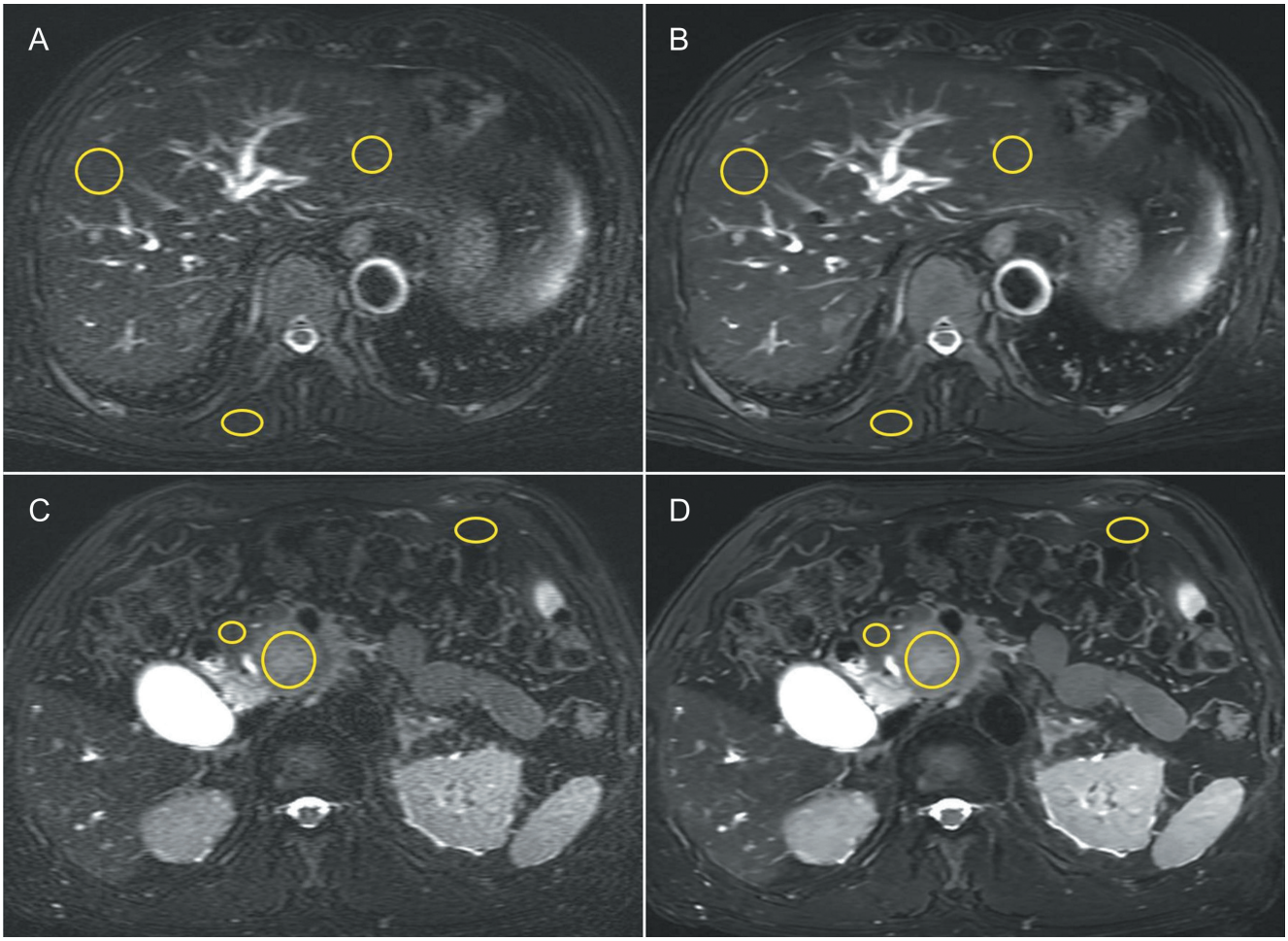

Fig. 1 ROI placements on SSFSE 3 mm images without (**A**, **C**) and with (**B**, **D**) DLIR algorithm. ROIs are manually drawn on the liver, pancreas, pancreatic cancer, paraspinal muscle, and intra-abdominal fat (circles). DLIR, deep learning image reconstruction; SSFSE, single-shot fast-spin echo.

suppression homogeneity, and overall image quality were assessed using a 5-point scale (1 = undiagnostic; 2 = suboptimal; 3 = acceptable; 4 = good; 5 = excellent). The images were presented in random order with preset windows, and the reader could adjust the window settings.

Statistical analysis

Continuous variables are expressed as mean ± SD. For quantitative analysis, the Shapiro–Wilk test was used to confirm the normality of the data distribution. Intraobserver agreements in SIs were assessed by using intraclass correlation coefficient (ICC; one-way random single measures) values. The SIs and SNRs of each object were compared for each T2-weighted sequence (FSE 6 mm, SSFSE 6 mm, and SSFSE 3 mm) with and without DLIR using a paired t-test. Pancreas-to-lesion contrasts were compared among the three T2-weighted sequences with DLIR using the Friedman test, followed by a post-hoc pairwise comparison using Dunn's multiple comparison test.

For the qualitative analysis, the inter-reader agreement was calculated using Cohen's weighted kappa statistics. The kappa values were stratified qualitatively by scores (0.00–0.20, poor; 0.21–0.40, fair; 0.41–0.60, moderate; 0.61–0.80, good; and 0.81–0.99, almost perfect). The Friedman test, followed by a post-hoc pairwise comparison with Dunn's test, was performed for multiple comparisons. Statistical analyses were performed using GraphPad Prism9. Statistical significance was set at a two-sided $P < 0.05$ for all the statistical analyses.

Results

Quantitative image analysis

The SIs were similar between the three T2-weighted sequences with and without DLIR in all the objects, although the SIs were slightly but significantly smaller on the images with DLIR than those on images without DLIR ($P < 0.001$) (Table 2). The measured SIs showed excellent agreements on the three T2-weighted images with and without DLIR in all

Table 2 SIs and SNRs of each object with and without DLIR on the three T2-weighted sequences

	FSE 6 mm			SSFSE 6 mm			SSFSE 3 mm		
	without DLIR	with DLIR	*P* value	without DLIR	with DLIR	*P* value	without DLIR	with DLIR	*P* value
Right liver lobe									
SI	409.2 ± 101.4	407.9 ± 101.9	<0.001	358.8 ± 96.3	355.7 ± 97.0	<0.001	350.9 ± 90.2	340.7 ± 93.3	<0.001
ICC	0.950	0.951		0.942	0.943		0.912	0.918	
SNR	9.3 ± 2.9	13.6 ± 5.1	<0.001	6.7 ± 2.4	11.0 ± 5.2	<0.001	4.3 ± 1.3	9.3 ± 4.0	<0.001
Left liver lobe									
SI	300.1 ± 85.0	299.0 ± 85.0	<0.001	266.1 ± 77.1	264.2 ± 77.2	<0.001	260.2 ± 79.2	253.9 ± 79.4	<0.001
ICC	0.909	0.910		0.867	0.870		0.843	0.860	
SNR	8.0 ± 2.9	9.8 ± 4.0	<0.001	6.4 ± 2.3	9.0 ± 4.1	<0.001	4.5 ± 1.7	7.9 ± 3.7	<0.001
Pancreas									
SI	632.5 ± 212.1	631.6 ± 212.3	<0.001	655.8 ± 319.9	654.1 ± 319.7	<0.001	638.0 ± 338.1	633.5 ± 339.3	<0.001
ICC	0.933	0.934		0.916	0.917		0.962	0.962	
SNR	10.2 ± 2.5	12.3 ± 4.0	<0.001	8.7 ± 2.2	11.6 ± 4.3	<0.001	6.7 ± 1.5	11.1 ± 3.9	<0.001
Pancreatic cancer									
SI	780.5 ± 180.7	779.5 ± 180.6	<0.001	847.9 ± 208.1	846.7 ± 208.0	<0.001	849.7 ± 195.5	846.1 ± 195.4	<0.001
ICC	0.857	0.857		0.831	0.830		0.867	0.870	
SNR	11.3 ± 2.4	12.6 ± 3.2	<0.001	10.2 ± 2.2	12.0 ± 3.1	<0.001	7.9 ± 1.9	11.0 ± 4.0	<0.001
Paraspinal muscle									
SI	268.9 ± 42.6	268.4 ± 42.6	<0.001	257.2 ± 43.1	255.7 ± 43.1	<0.001	243.5 ± 40.3	239.8 ± 41.0	<0.001
ICC	0.941	0.942		0.913	0.913		0.918	0.917	
SNR	10.5 ± 2.5	13.6 ± 4.1	<0.001	7.5 ± 1.6	11.6 ± 3.8	<0.001	5.4 ± 1.1	11.0 ± 3.3	<0.001
Intra-abdominal fat									
SI	196.5 ± 57.2	195.6 ± 57.3	<0.001	179.4 ± 80.6	179.4 ± 80.6	<0.001	167.5 ± 66.9	157.8 ± 65.5	<0.001
ICC	0.868	0.870		0.858	0.856		0.869	0.866	
SNR	5.7 ± 2.0	7.3 ± 2.9	<0.001	3.9 ± 1.1	5.7 ± 2.1	<0.001	2.9 ± 0.8	5.3 ± 2.1	<0.001

Measurement data are presented as mean ± standard deviation. DLIR, deep learning image reconstruction; FSE, fast spin echo; ICC, intraclass correlation coefficient; SSFSE, single-shot fast spin echo; SI, signal intensity.

the objects. The SNRs significantly improved in the three T2-weighted sequences with DLIR compared to those without DLIR in all the objects ($P < 0.001$) (Fig. 2). The SNRs increase% for the SSFSE 3 mm was higher for all the objects than those for FSE 6 mm and SSFSE 6 mm (Table 3). With DLIR, the SNRs increased by 19%, 30%, and 63% in the pancreas and by 11%, 17%, and 36% in pancreatic cancer for FSE 6 mm, SSFSE 6 mm, and SSFSE 3 mm, respectively.

Pancreas-to-lesion contrasts on FSE 6 mm, SSFSE 6 mm, and SSFSE 3 mm with DLIR were 0.30 ± 0.33, 0.46 ± 0.50, and 0.52 ± 0.49, respectively (Fig. 3). The pancreas-to-lesion contrast of SSFSE at 3 mm was higher than that of FSE 6 mm ($P < 0.001$) and tended to be higher than SSFSE 6 mm ($P = 0.07$), and that of SSFSE at 6 mm was higher than that of FSE at 6 mm ($P = 0.03$).

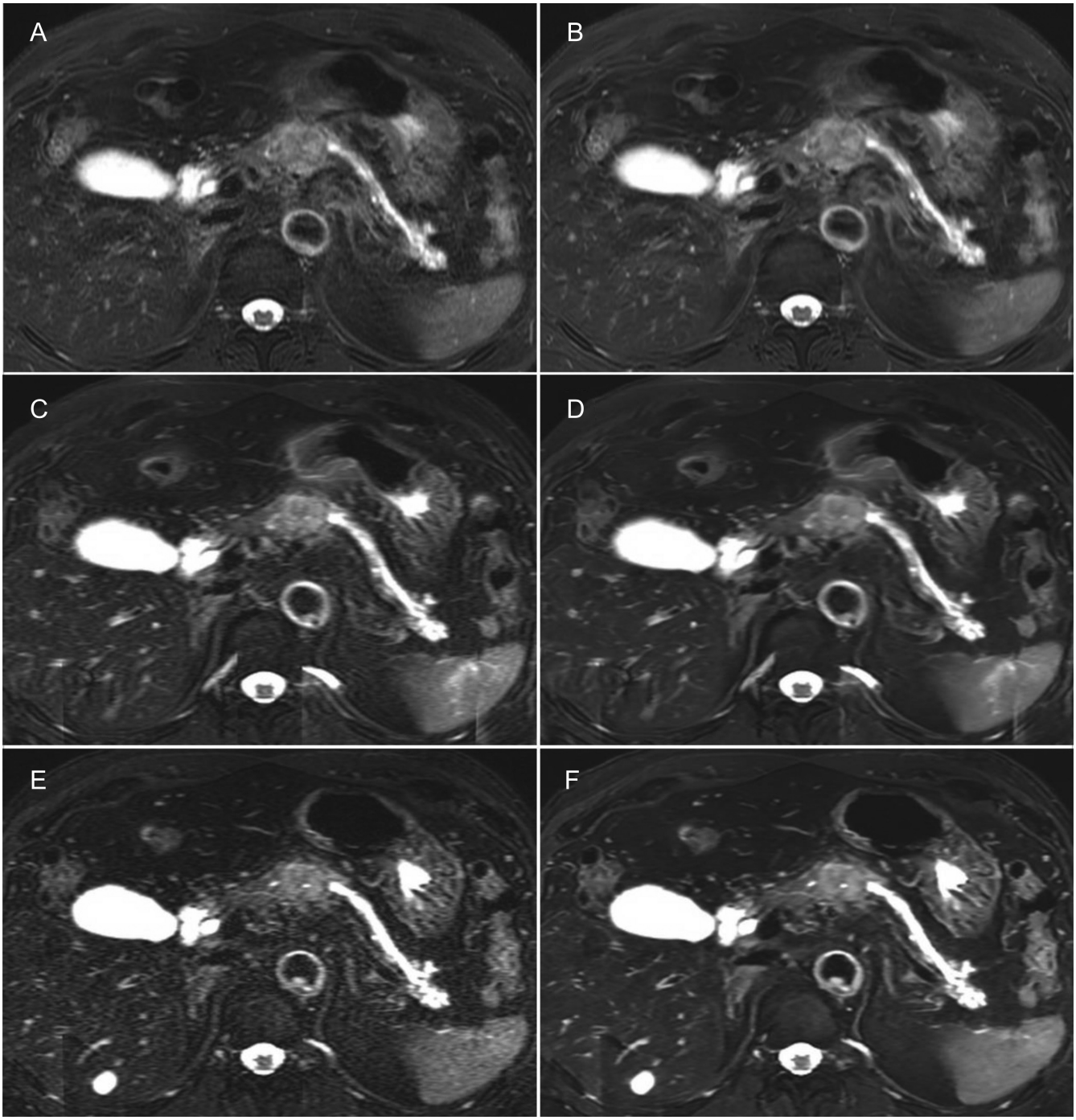

Fig. 2 Axial T2-weighted images in a 68-year-old man with pancreatic ductal adenocarcinoma of the pancreas head. DLIR reduces image noise among (**B**) FSE 6 mm, (**D**) SSFSE 6 mm, and (**F**) SSFSE 3 mm compared with (**A**) FSE 6 mm, (**C**) SSFSE 6 mm, and (**E**) SSFSE 3 mm without implementation of DLIR. The main pancreatic duct is more clearly visualized, and pancreas edge sharpness is more evident on SSFSE 3 mm with DLIR than on FSE 6 mm with DLIR and SSFSE 6 mm with DLIR. DLIR, deep learning image reconstruction; FSE, fast-spin echo; SSFSE, single-shot fast-spin echo.

Qualitative image analysis

The results of the qualitative analysis are presented in Table 4. The SSFSE 3 mm with DLIR had significantly high image qualities regarding pancreas edge sharpness, pancreatic duct clarity, and overall image quality, followed by SSFSE 6 mm with DLIR and FSE 6 mm with DLIR ($P < 0.001$). For respiratory motion artifacts, SSFSE 3 mm with DLIR and SSFSE 6 mm with DLIR were significantly better

Table 3 SNR increase% of each object on the three T2-weighted sequences with DLIR

	FSE 6 mm	SSFSE 6 mm	SSFSE 3 mm
Right liver lobe	143.4 ± 19.5%	160.5 ± 25.1%	207.9 ± 40.7%
Left liver lobe	122.6 ± 12.3%	138.2 ± 20.3%	170.9 ± 33.7%
Pancreas	118.8 ± 13.0%	130.4 ± 21.8%	162.8 ± 37.7%
Pancreatic cancer	111.3 ± 7.2%	116.9 ± 10.4%	136.4 ± 22.4%
Paraspinal muscle	127.9 ± 14.0%	152.6 ± 26.4%	202.5 ± 40.3%
Intra-abdominal fat	127.5 ± 14.8%	142.6 ± 26.8%	177.1 ± 41.3%

Measurement data are presented as mean ± standard deviation. FSE, fast spin-echo; SSFSE, single-shot fast spin-echo.

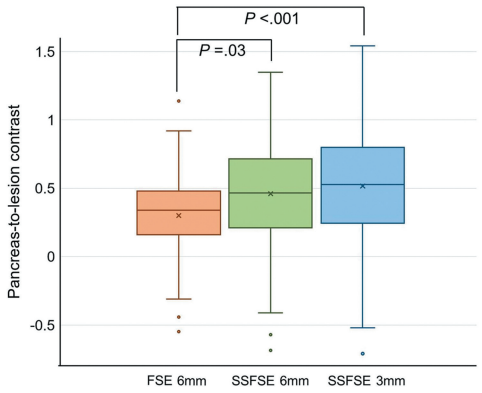

Fig. 3 Box plots showing pancreas-to-lesion contrast on the FSE 6 mm, SSFSE 6 mm, and SSFSE 3 mm images with DLIR. The lower boundary of the boxes indicates the 25th percentile, the line within the boxes indicates the median, and the higher boundary of the boxes indicates the 75th percentile. DLIR, deep learning image reconstruction; FSE, fast-spin echo; SSFSE, single-shot fast-spin echo.

than FSE 6 mm with DLIR, and no significant differences were observed between the SSFSE 6 mm with DLIR and FSE 6 mm with DLIR (Fig. 4). The lesion conspicuity scores of SSFSE 3 mm with DLIR were significantly higher than those of FSE 6 mm with DLIR ($P < 0.001$), but comparable with SSFSE 6 mm with DLIR. The fat suppression homogeneity tended to have a high quality on SSFSE 3 mm with DLIR, followed by SSFSE 6 mm with DLIR and was similar between SSFSE 6 mm with DLIR and SSFSE 3 mm with DLIR. The inter-reader agreements were 0.52–0.63 for respiratory motion artifact, 0.66–0.74 for pancreas edge sharpness, 0.59–0.78 for pancreatic duct clarity, 0.52–0.77 for lesion conspicuity, 0.57–0.64 for fat suppression homogeneity, and 0.71–0.81 for overall image quality (Table 5).

Discussion

We investigated the utility of SSFSE 3 mm and SSFSE 6 mm pulse sequences with DLIR compared to that of the conventional FSE 6 mm sequence with DLIR for pancreatic cancer. The commercial DLIR significantly improved the SNRs on the three T2WI in the upper abdominal organs. The SSFSE 3 mm was superior to SSFSE 6 mm and FSE 6 mm in improving SNR and subjective image quality. These results indicated that thin-slice SSFSE with DLIR can improve the SNR and image quality, providing better visualization of pancreatic cancer and upper abdominal organs than does conventional FSE.

The SNRs of the upper abdominal organs were significantly higher on the three T2W sequences with DLIR than on those without DLIR, which concurs with the results of previous studies.[12,15–18] Our results showed that the noise reduction by applying DLIR was more effective on thin-slice SSFSE 3 mm images than on conventional FSE 6 mm and SSFSE 6 mm images. Additionally, SNRs on the SSFSE 3 mm with DLIR were similar to those on the FSE 6 mm without DLIR regarding the pancreas and pancreatic cancer, and the pancreas-to-lesion contrast was significantly greater on FSE 3 mm with DLIR than on the other T2WIs. Therefore, thin-slice fat-suppressed SSFSE imaging could be an option for evaluating pancreatic cancer and warrant further investigation. Meanwhile, the SI values were slightly but significantly smaller for the three T2-weighted sequences with DLIR than for those without DLIR. This might be because DLIR intentionally reduces truncation artifacts and Gibb's overshoot signal on the edges of the image objects.

The SSFSE is characterized by relatively fewer motion artifacts but a lower SNR than those for FSE images when the same spatial resolution is applied.[6–8] However, DLIR has addressed the concern of a lower SNR for SSFSE, which was clarified by our results and those of previous studies.[13,15–17] There were fewer respiratory motion artifacts on SSFSE images than on FSE images in this study. The improvement in motion artifacts may be attributed to the smaller number of breath holds, which is an advantage of a single-shot T2-weighted sequence.[6–8] Although current DLIR algorithms do not eliminate the motion artifacts, previous studies have also shown fewer motion artifacts on single-shot T2WI than on FSE T2WI.[15–17] We found that the overall image quality was significantly higher on SSFSE images than on FSE images, which can be explained by the comprehensive

Table 4 Qualitative image analyses on the three T2-weighted sequences with DLIR

	FSE 6 mm	SSFSE 6 mm	SSFSE 3 mm	*P* values			
					FSE 6 mm vs. SSFSE 6 mm	FSE 6 mm vs. SSFSE 3 mm	SSFSE 6 mm vs. SSFSE 3 mm
Respiratory motion artifacts							
Reader 1	2.9 ± 1.1	3.8 ± 0.7	4.3 ± 0.7	<0.001	<0.001	<0.001	0.07
Reader 2	3.4 ± 0.9	4.3 ± 0.6	4.4 ± 0.5	<0.001	<0.001	<0.001	0.99
Pancreas edge sharpness							
Reader 1	3.2 ± 1.1	3.9 ± 0.8	4.5 ± 0.6	<0.001	<0.001	<0.001	0.002
Reader 2	3.1 ± 0.9	4.0 ± 0.8	4.2 ± 0.8	<0.001	<0.001	<0.001	0.69
Pancreatic duct clarity							
Reader 1	3.2 ± 0.8	4.3 ± 0.8	4.8 ± 0.4	<0.001	<0.001	<0.001	0.03
Reader 2	3.1 ± 0.9	4.3 ± 0.7	4.6 ± 0.6	<0.001	<0.001	<0.001	0.47
Lesion conspicuity							
Reader 1	3.6 ± 1.3	4.1 ± 1.0	4.4 ± 0.8	<0.001	0.11	<0.001	0.24
Reader 2	3.2 ± 0.9	4.1 ± 0.8	4.5 ± 0.6	<0.001	<0.001	<0.001	0.34
Fat suppression homogeneity							
Reader 1	4.2 ± 0.8	4.4 ± 0.7	4.5 ± 0.6	<0.001	0.99	0.19	0.99
Reader 2	3.7 ± 0.8	4.2 ± 0.7	4.3 ± 0.7	<0.001	0.03	0.002	0.99
Overall image quality							
Reader 1	3.1 ± 0.8	4.0 ± 0.9	4.6 ± 0.5	<0.001	<0.001	<0.001	0.01
Reader 2	3.1 ± 0.6	4.2 ± 0.7	4.6 ± 0.6	<0.001	<0.001	<0.001	0.13

Measurement data are presented as mean ± standard deviation. FSE, fast spin-echo; SSFSE, single-shot fast spin-echo.

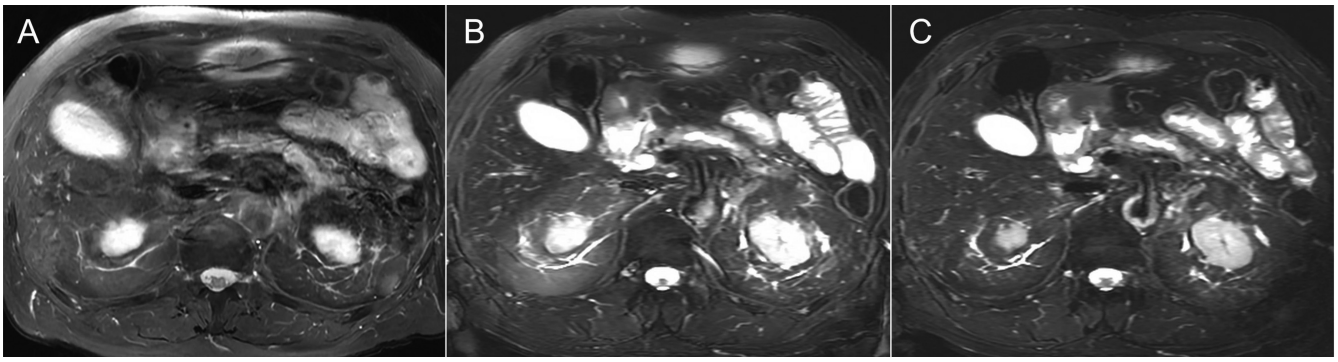

Fig. 4 Axial T2-weighted images in a 73-year-old man with pancreatic ductal adenocarcinoma of the pancreas head (not depicted in these slices). Substantial motion artifacts from the gastrointestinal tract deteriorate image quality on (**A**) FSE 6 mm with DLIR. A decrease in the motion artifacts improves visualization of the pancreas on (**B**) SSFSE 6 mm and (**C**) SSFSE 3 mm with DLIR. DLIR, deep learning image reconstruction; FSE, fast-spin echo; SSFSE, single-shot fast-spin echo.

improvements in single-shot T2-weighted sequences using DLIR.

The clinical utility of DLIR on thin-slice T2WI of the upper abdomen has not been fully investigated. In our study, pancreas edge sharpness and pancreatic duct clarity were substantially higher on SSFSE 3 mm than on FSE 6 mm and SSFSE 6 mm, which was prominently different from the results in previous studies investigating the improvement of image quality on single-shot T2WI with DLIR of the liver.[15–17] This may be because the pancreas is

Table 5 Inter-reader agreement for qualitative image analyses on the three T2-weighted sequences with DLIR

	FSE 6 mm	SSFSE 6 mm	SSFSE 3 mm
Respiratory motion artifacts	0.52 (0.39, 0.73)	0.53 (0.36, 0.70)	0.63 (0.42, 0.80)
Pancreas edge sharpness	0.71 (0.59, 0.84)	0.74 (0.62, 0.84)	0.66 (0.46, 0.79)
Pancreatic duct clarity	0.59 (0.39, 0.70)	0.78 (0.63, 0.89)	0.71 (0.55, 0.81)
Lesion conspicuity	0.52 (0.39, 0.72)	0.72 (0.58, 0.81)	0.77 (0.63, 0.88)
Fat suppression homogeneity	0.57 (0.37, 0.76)	0.59 (0.37, 0.71)	0.64 (0.43, 0.82)
Overall image quality	0.72 (0.57, 0.85)	0.71 (0.53, 0.82)	0.81 (0.68, 0.91)

Numbers in parentheses represent 95% confidence intervals. FSE, fast spin-echo; SSFSE, single-shot fast spin-echo.

a thin and small organ surrounded by the gastrointestinal tract and is more highly affected by motion artifacts than is the liver. The thin-slice SSFSE, which provides motion resistance and a minimal partial volume effect, would be useful for evaluating the pancreas because of the clear visualization of the pancreatic edge and duct. Moreover, the development of MRI hardware and implementation of DLIR allow for variable refocusing flip angles and full-Fourier acquisition while achieving clinically relevant effective echo times, which improve the image sharpness and intermediate T2 signal contrast.[7] We believe that the thin-slice fat-suppressed SSFSE with DLIR used in this study can be a reliable sequence for the simultaneous detailed assessment of pancreatic parenchymal and ductal structures and neoplastic lesions.

Our study had some limitations. First, this was a single-institution retrospective study with a relatively small number of patients. However, significant differences were observed in most analyses, and similar results are expected even in studies with a larger number of patients. Second, the comparisons among other T2-weighted sequences, such as respiratory-triggered T2WI and motion-robust T2WI, were not performed.[13,15–17] Further studies are needed to determine whether SSFSE with DLIR can be used instead of T2-weighted sequences. Third, we did not evaluate the diagnostic performance of the proposed method for detecting and characterizing pancreatic lesions, which warrants further clinical investigation. Finally, this study employed only a single-vendor MRI scanner, and whether the results can be replicated using other MRI scanners needs to be determined in future studies using other MRI scanners that employ different DLIR algorithms.

In conclusion, the SSFSE of 3 mm with DLIR demonstrated significant improvements in the SNRs of the pancreas, pancreas-to-lesion contrast, and image quality compared with those of the SSFSE of 6 mm and FSE of 6 mm. The thin-slice fat-suppressed single-shot T2WI with DLIR can be easily implemented for pancreatic MR protocol.

Conflicts of Interest

Tetsuya Wakayama is an employee of GE Healthcare. Takamichi Murakami has financial supports for research fundings from Guerbet Japan and Siemens Healthineers. The remaining authors declare no conflicts of interest directly relevant to the content of this article.

References

1. Lee SS, Byun JH, Hong HS, et al. Image quality and focal lesion detection on T2-weighted MR imaging of the liver: Comparison of two high-resolution free-breathing imaging techniques with two breath-hold imaging techniques. *J Magn Reson Imaging* 2007; 26:323–330.
2. Klessen C, Asbach P, Kroencke TJ, et al. Magnetic resonance imaging of the upper abdomen using a free-breathing T2-weighted turbo spin echo sequence with navigator triggered prospective acquisition correction. *J Magn Reson Imaging* 2005; 21:576–582.
3. Schreiber-Zinaman J, Rosenkrantz AB. Frequency and reasons for extra sequences in clinical abdominal MRI examinations. *Abdom Radiol (NY)* 2017; 42:306–311.
4. Hirokawa Y, Isoda H, Maetani YS, Arizono S, Shimada K, Togashi K. Evaluation of motion correction effect and image quality with the periodically rotated overlapping parallel lines with enhanced reconstruction (PROPELLER) (BLADE) and parallel imaging acquisition technique in the upper abdomen. *J Magn Reson Imaging* 2008; 28:957–962.
5. Rosenkrantz AB, Patel JM, Babb JS, Storey P, Hecht EM. Liver MRI at 3 T using a respiratory-triggered time-efficient 3D T2-weighted technique: Impact on artifacts and image quality. *AJR Am J Roentgenol* 2010; 194:634–641.
6. Semelka RC, Kelekis NL, Thomasson D, Brown MA, Laub GA. Haste MR imaging: Description of technique and preliminary results in the abdomen. *J Magn Reson Imaging* 1996; 6:698–699.
7. Loening AM, Litwiller DV, Saranathan M, Vasanawala SS. Increased speed and image quality for pelvic single-shot fast spin-echo imaging with variable refocusing flip angles and Full-Fourier acquisition. *Radiology* 2017; 282:561–568.
8. Hicks RM, Loening AM, Ohliger MA, Vasanawala SS, Hope TA. Variable refocusing flip angle single-shot fast spin echo imaging of liver lesions: Increased speed and lesion contrast. *Abdom Radiol (NY)* 2018; 43:593–599.
9. Kim BS, Kim JH, Choi GM, et al. Comparison of three free-breathing T2-weighted MRI sequences in the evaluation of focal liver lesions. *AJR Am J Roentgenol* 2008; 190:W19–W27.
10. Schwartz LH, Seltzer SE, Tempany CM, et al. Prospective comparison of T2-weighted fast spin-echo, with and without

fat suppression, and conventional spin-echo pulse sequences in the upper abdomen. *Radiology* 1993; 189:411–416.
11. Tirkes T, Menias CO, Sandrasegaran K. MR imaging technique for pancreas. *Radiol Clin North Am* 2012; 50:379–393.
12. Sheng RF, Zheng LY, Jin KP, et al. Single-breath-hold T2WI liver MRI with deep learning-based reconstruction: A clinical feasibility study in comparison to conventional multi-breath-hold T2WI liver MRI. *Magn Reson Imaging* 2021; 81:75–81.
13. Herrmann J, Gassenmaier S, Nickel D, et al. Diagnostic confidence and feasibility of a deep learning accelerated HASTE sequence of the abdomen in a single breath-hold. *Invest Radiol* 2021; 56:313–319.
14. Herrmann J, Nickel D, Mugler JP III, et al. Development and evaluation of deep learning-accelerated single-breath-hold abdominal HASTE at 3T using variable refocusing flip angles. *Invest Radiol* 2021; 56:645–652.
15. Shanbhogue K, Tong A, Smereka P, et al. Accelerated single-shot T2-weighted fat-suppressed (FS) MRI of the liver with deep learning-based image reconstruction: Qualitative and quantitative comparison of image quality with conventional T2-weighted FS sequence. *Eur Radiol* 2021; 31:8447–8457.
16. Tajima T, Akai H, Yasaka K, et al. Clinical feasibility of an abdominal thin-slice breath-hold single-shot fast spin echo sequence processed using a deep learning-based noise-reduction approach. *Magn Reson Imaging* 2022; 90:76–83.
17. Ichinohe F, Oyama K, Yamada A, et al. Usefulness of breath-hold fat-suppressed T2-weighted images with deep learning-based reconstruction of the liver: Comparison to conventional free-breathing turbo spin echo. *Invest Radiol* 2023; 58:373–379.
18. Zhang Y, Peng W, Xiao Y, et al. Rapid 3D breath-hold MR cholangiopancreatography using deep learning-constrained compressed sensing reconstruction. *Eur Radiol* 2023; 33:2500–2509.
19. Lebel RM. Performance characterization of a novel deep learning-based MR image reconstruction pipeline. arXiv:2008.06559; 2020.
20. Kiso K, Tsuboyama T, Onishi H, et al. Effect of deep learning reconstruction on respiratory-triggered T2-weighted MR imaging of the liver: A comparison between the single-shot fast spin-echo and fast spin-echo sequences. *Magn Reson Med Sci* 2024; 23:214–224.